CrossMark

The effect of rib shape on the behavior of laminar flow of oil/MWCNT nanofluid in a rectangular microchannel

Mohammad Reza Gholami[1] · Omid Ali Akbari[2] · Ali Marzban[1] ·
Davood Toghraie[3] · Gholamreza Ahmadi Sheikh Shabani[2] · Majid Zarringhalam[4]

Abstract

In this research, the laminar and forced flow and heat transfer of oil/multi-walled carbon nanotubes nanofluid in a microchannel have been numerically investigated. The studied geometrics is a two-dimensional rectangular microchannel with the proportion of length to height of 150 ($L/d = 150$). The purpose of this research is to investigate the effect of using rectangular, oval, parabolic, triangular and trapezoidal rib shapes on behavior and heat transfer of nanofluid flow in the rectangular microchannel. This research has been simulated in Reynolds numbers of 1, 10, 50 and 100 and volume fractions of 0, 2 and 4% of nanoparticles by using finite volume method. The results of this research indicate that the existence of ribs enhances the friction factor and Nusselt number, significantly. Also, the shape of rib is one of the most important factors for determining the behavior and heat transfer of cooling fluid flows. Among the investigated rib shapes, the parabolic rib, comparing to the augmentation of friction factor, has the best proportion of Nusselt number enhancement.

List of symbols

A	Area (m^2)
f	Friction factor
C_p	Heat capacity (Jkg^{-1} K^{-1})
D	Microchannel height (μm)
H	Ribbed height (m)
k	Thermal conductivity coefficient (Wm^{-1} K^{-1})
K	Inlet microchannel length (m)
L	Microchannel length (m)
M	Ribbed length (m)
Nu	Nusselt number
P	Fluid pressure (Pa)
p	Ribbed pitch (m)
Pe	Peclet number
$Pr = (v_f)/\alpha_f$	Prandtl number
$Re = (\rho_f u H)/\mu_f$	Reynolds number
T	Temperature (K)
U, V	Dimensionless velocity components in x, y directions
X, Y	Cartesian dimensionless coordinates
u, v	Velocity components in x, y directions (ms^{-1})
u_c	Inlet velocity in x directions (ms^{-1})
u_s	Brownian motion velocity (ms^{-1})
W	Outlet microchannel length (m)

Greek symbols

α	Thermal diffusivity (m^2 s^{-1})
φ	Nanoparticles volume fraction
κb	Boltzmann constant (JK^{-1})
μ	Dynamic viscosity (Pa s)
θ	Dimensionless temperature
ρ	Density (kg m^{-3})
υ	Kinematics viscosity (m^2 s^{-1})

✉ Davood Toghraie
Toghraee@iaukhsh.ac.ir

1 Department of Mechanical Engineering, Aligoudarz Branch, Islamic Azad University, Aligoudarz, Iran

2 Young Researchers and Elite Club, Khomeinishahr Branch, Islamic Azad University, Khomeinishahr, Iran

3 Department of Mechanical Engineering, Khomeinishahr Branch, Islamic Azad University, 84175-119 Khomeinishahr, Iran

4 Young Researchers and Elite Club, South Tehran Branch, Islamic Azad University, Tehran, Iran

Super- and subscripts

c	Cold
Eff	Effective
f	Base fluid (oil)
h	Hot
Ave	Average
Nf	Nanofluid
s	Solid nanoparticles

Introduction

Today, the heat transfer enhancement in volume unites the transformation of heat transfer sections and the changes of boundary conditions are some of the important factors in different fields of heat transfer. In recent years [1–13], producing compact heating systems has become a basic and challenging purpose for obtaining higher efficiency in different industries. According to some previous studies, to increase the produced power in some power plants, or to some upgrading, there is an emergency need to increase the heat transfer capacity in existing systems [14–20]. One of the best solutions for this problem is using nanofluids instead of water in this cooling system. Among the effective methods, adding metallic and nonmetallic particles to the base fluid, called nanofluid, has become an innovative and impressive method for heat transfer enhancement. In fact, nanofluids are a new generation of fluids with higher potentiality and efficiency in the industrial applications. Recent studies have revealed that unlike the fluids, nanofluids have significant rate of heat transfer enhancement [21–34]; therefore, in novel equipment, the heat transfer issue has high importance among the researchers using this science. By combining some methods such as using nanofluids and microchannels with other methods, the researchers have improved the efficiency of heat transfer equipment. Behnampour et al. [35] numerically investigated the effect of using rectangular, triangular and trapezoidal ribs on behavior and laminar heat transfer of water/AgO nanofluid flow with nanoparticles volume fractions of 0–4% in a rectangular microchannel. His results demonstrated that the rectangular rib causes the most changes of velocity profile in the central line of flow and the triangular rib has the best rate of performance evaluation criterion. Akbari et al. [36] numerically studied the effect of rib height changes on flow and laminar heat transfer of water/Al₂O₃ nanofluid in a two-dimensional microchannel. He figures out that, by increasing rib height, Reynolds number and volume fraction of nanoparticles, the rate of heat transfer improves. In another research, the effect of rectangular rib on the behavior and laminar heat transfer of water/Al₂O₃ nanofluid flow in a three-dimensional rectangular microchannel has been studied by

Akbari et al. [37]. His numerical results demonstrated that, by increasing Reynolds number, rib number and volume fraction of nanoparticles, the heat transfer on the heated surfaces improves. Karimipour et al. [38] simulated the effect of using rectangular rib on the forced heat transfer of water/Ag nanofluid in a rectangular microchannel under the constant thermal boundary condition. His numerical results indicated that, in higher Reynolds numbers, by increasing volume fraction of nanoparticles and rib number, Nusselt number enhances significantly. Gravandyan et al. [39], by using rectangular ribs with different pitches, studied the effective factors on flow structure and heat transfer of water/TiO₂ in a two-dimensional microchannel. He figured out that sudden changes of fluid flow velocity in the microchannel have different effects on friction factor behavior, and by increasing Reynolds number, these effects become more considerable. Also, in the indented zones, the enhancement of AR ratio has a great effect on the depreciation of fluid momentum. Although numerous studies have been done in heat transfer field, due to the advantages of using nanofluids in different geometrics [40–48], investigating heat transfer mechanisms is continuous. In this paper, the effect of using rectangular, triangular, trapezoidal, oval and parabolic ribs has been simulated in a two-dimensional rectangular microchannel with constant heat flux boundary condition. In order to improve the heat transfer in the studied microchannel, oil/MWCNT has been used in different volume fractions. The effect of simultaneous use of nanofluid, minimized dimensions, the existence of rib with different forms, numerical simulation of flow parameters and the forced and laminar heat transfer with the mentioned properties have made the present research more advantageous. The results of present numerical simulation have been compared by different values of volume fraction of nanoparticles, Reynolds numbers and rib shapes.

Problem statement and geometrical dimensions

The present study has been simulated in a two-dimensional rectangular microchannel with the length of $L = 7.5$ mm and the height of $d = 50$ μm. The top wall with the length of L and the bottom wall with the length of $K = 3.75$ mm are insulated from the inlet area. The rest of the bottom wall of microchannel with the length of $L–K = 3.75$ mm is under the constant heat flux of $q'' = 10{,}000$ W m^{-2}. The inlet temperature of cooling fluid is constant and $T_c = 298$ K. Oil and the nanoparticles of MWCNT are in thermal equilibrium. This research has been done in Reynolds numbers of 1, 10, 50 and 100 and volume fractions of 0, 2 and 4% of solid nanoparticles and for the rectangular,

oval, parabolic, triangular and trapezoidal rib shapes. In order to have better comparison for each rib shape described in this research, the height (H) and the length of rib (m) have been considered as constant. Figure 1 indicates the considered geometrics of the present research.

In Fig. 1, p is the pitch of rib, H is rib height, d is the height of microchannel, L is the length of microchannel, K is the inlet length of microchannel, m is the width of rib, and w is the outlet length of microchannel. In this research, the numerical simulation of heat transfer and nanofluid flow inside the mentioned microchannel has been done for the rectangular, trapezoidal and triangular rib shapes. In this study, in order to have better investigation and accurate comparison of the numerical results in different rib shapes, in all of the states, p, H, m and w have been considered constant and, respectively, equal with $p = 300$ μm, $H = 20$ μm, $m = 100$ μm and $w = 2250$ μm. The molecular diameter of oil fluid is $d_f = 2$ Å, and the nanoparticles of carbon nanotubes are spherical and have uniform shape with the diameter of $d_p = 5$ nm [49]. The properties of oil fluid, MWCNT nanoparticles [49] and nanofluid with different volume fractions are presented in Table 1.

Governing equations of the two-dimensional laminar flow

The governing equations of flow and the forced, two-dimensional, laminar, constant and single-phase heat transfer including consistency, momentum and energy equations are as follows [50]:

$$\frac{\partial u}{\partial x} + \frac{\partial x}{\partial y} + \frac{\partial w}{\partial z} = 0 \tag{1}$$

$$u\frac{\partial u}{\partial x} + v\frac{\partial u}{\partial y} = -\frac{1}{\rho_{nf}}\frac{\partial p}{\partial x} + v_{nf}\left(\frac{\partial}{\partial x}\left(\frac{\partial u}{\partial x}\right) + \frac{\partial}{\partial y}\left(\frac{\partial u}{\partial y}\right)\right) \tag{2}$$

$$u\frac{\partial v}{\partial x} + v\frac{\partial v}{\partial y} = -\frac{1}{\rho_{nf}}\frac{\partial p}{\partial x} + v_{nf}\left(\frac{\partial}{\partial x}\left(\frac{\partial v}{\partial x}\right) + \frac{\partial}{\partial y}\left(\frac{\partial v}{\partial y}\right)\right) \tag{3}$$

$$u\frac{\partial T}{\partial x} + v\frac{\partial T}{\partial y} = \alpha_{nf}\left(\frac{\partial}{\partial x}\left(\frac{\partial T}{\partial x}\right) + \frac{\partial}{\partial y}\left(\frac{\partial T}{\partial y}\right)\right) \tag{4}$$

The equations related to the non-dimensioning of governing equations of laminar and forced nanofluid flow are described as follows [51]:

$$X = \frac{x}{H}, \quad Y = \frac{y}{H}, \quad U = \frac{u}{u_c}, \quad V = \frac{v}{u_c}, \quad P = \frac{\bar{P}}{\rho_{nf}u_c^2},$$
$$\theta = \frac{T - T_c}{\Delta T}, \quad Re = \frac{u_c \times H}{v_f}, \quad Pr = \frac{v_f}{\alpha_f}, \quad \Delta T = \frac{q''D_h}{k_f} \tag{5}$$

By substituting the dimensionless Eq. (5) in Eqs. (1–4), the consistency, momentum and energy equations in the dimensionless state can be written as follows [52]:

$$\frac{\partial U}{\partial X} + \frac{\partial V}{\partial Y} = 0 \tag{6}$$

$$U\frac{\partial U}{\partial X} + V\frac{\partial U}{\partial Y} = -\frac{\partial P}{\partial X} + \frac{\mu_{nf}}{\rho_{nf}v_f}\frac{1}{Re}\left(\frac{\partial^2 U}{\partial X^2} + \frac{\partial^2 U}{\partial Y^2}\right) \tag{7}$$

$$U\frac{\partial V}{\partial X} + V\frac{\partial V}{\partial X} = -\frac{\partial P}{\partial Y} + \frac{\mu_{nf}}{\rho_{nf}v_f}\frac{1}{Re}\left(\frac{\partial^2 V}{\partial X^2} + \frac{\partial^2 V}{\partial Y^2}\right) \tag{8}$$

$$U\frac{\partial \theta}{\partial X} + V\frac{\partial \theta}{\partial Y} = \frac{\alpha_{nf}}{\alpha_f}\frac{1}{RePr}\left(\frac{\partial^2 \theta}{\partial X^2} + \frac{\partial^2 \theta}{\partial Y^2}\right) \tag{9}$$

The dimensionless boundary conditions for the studied geometrics of the present paper are defined as follows:

$$U = 1, \quad V = 0 \text{ and } \theta = 0 \quad \text{for } X = 0 \text{ and } 0 \leq Y \leq 1 \tag{10}$$

$$V = 0 \text{ and } \frac{\partial U}{\partial X} = 0 \text{ for } X = 150 \text{ and } 0 \leq Y \leq 1 \tag{11}$$

$$U = 0, \quad V = 0 \text{ and } \frac{\partial \theta}{\partial Y} = 0 \text{ for } Y = 1 \text{ and } 0 \leq X \leq 150 \tag{12}$$

$$U = 0,$$
$$V = 0 \text{ and } \frac{\partial \theta}{\partial Y} = 0 \text{ or } \frac{\partial \theta}{\partial Y} = -\frac{k_f}{k_{nf}} \text{ for } Y \tag{13}$$
$$= 0 \text{ and } 0 \leq X \leq 150$$

The equations related to the computation of nanofluid properties and flow parameters

Following equations are used for calculating the density [53] and the specific heat capacity of nanofluid [54]:

$$\rho_{nf} = (l - \varphi)\rho_f + \varphi\rho_s \tag{14}$$

$$(\rho C_p)_{nf} = (l - \varphi)(\rho C_p)_f + \varphi(\rho C_p)_s \tag{15}$$

Chon equation [55] has been used for computing the thermal conductivity of nanofluid.

$$\frac{k_m}{k_f} = 1 + 64.7 \phi^{0.746}\left(\frac{d_f}{d_{np}}\right)^{0.369}\left(\frac{k_{np}}{k_f}\right)^{0.7476}Pr^{0.9955}Re^{1.2321}$$

$$Re = \frac{\rho_f k_b T}{3\pi\mu^2 l_f}, \quad Pr = \frac{\mu_f}{\rho_f\alpha_f}, \quad \mu = A \times 10^{\frac{B}{T-C}}, \quad C = 140(K),$$

$$B = 247(K), \quad A = 2.414 \times 10^{-5} \text{ (Pa.s)}, \quad T = T_{in} \tag{16}$$

In the above equations, the indexes of ρ, k, φ and C_p are, respectively, the density, thermal conductivity coefficient, volume fraction of nanoparticle and the specific heat capacity and the subindexes of s, f and nf are, respectively,
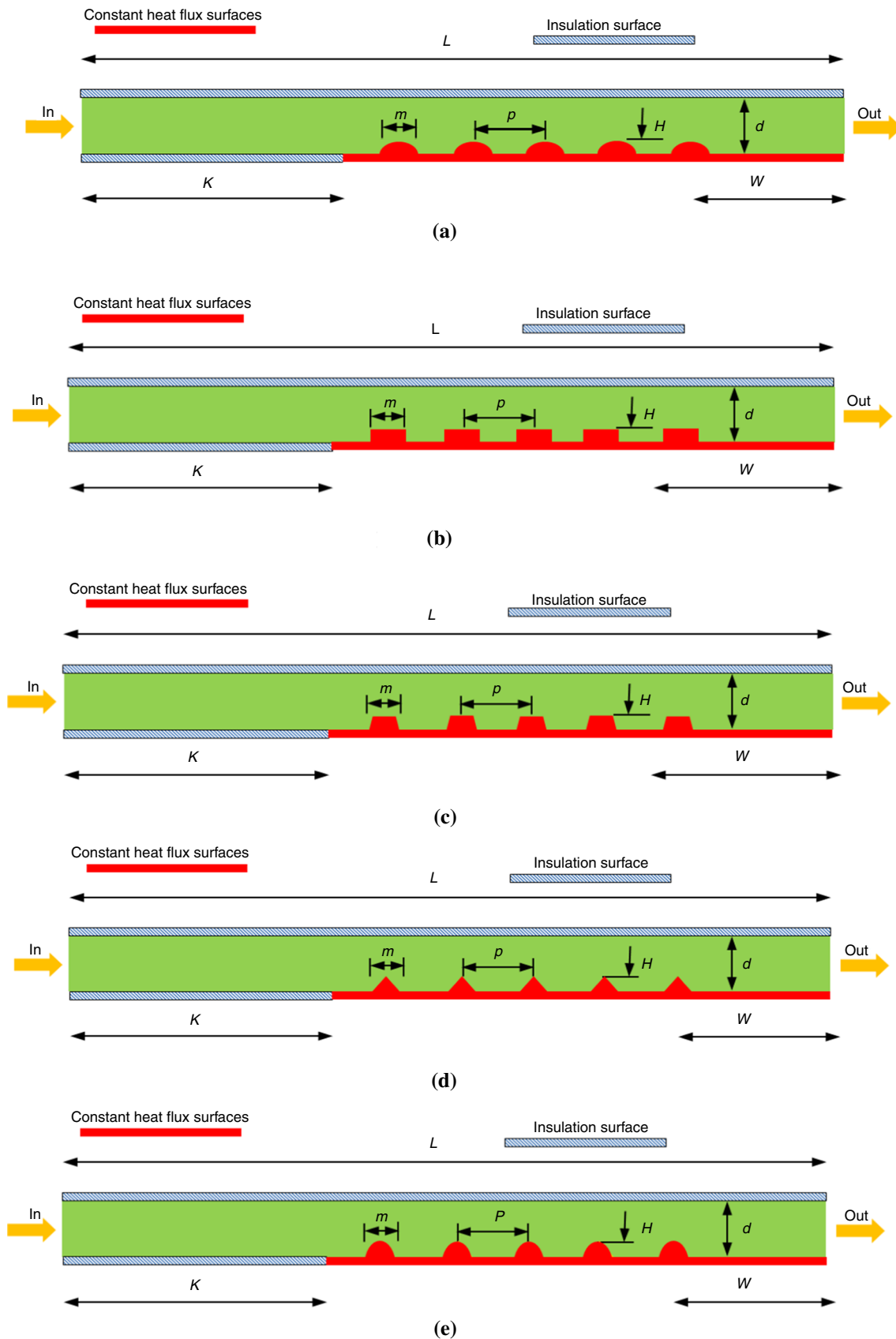
Fig. 1 The schematic of the studied microchannel. **a** Elliptical, **b** rectangular, **c** trapezoidal, **d** triangular, **e** parabolic

Table 1 The thermophysical properties of the base fluid and solid nanoparticles

	Oil [49]	MWCNT [49]	Nanofluid $\varphi = 0.02$	Nanofluid $\varphi = 0.04$
C_p/Jkg^{-1}K^{-1}	2032	1700	2012.9	1995.1
ρ/kgm^{-3}	2032	2600	901.66	936.32
k/Wm^{-1}K^{-1}	0.133	3000	0.5255	0.7912
μ/Pa s	0.0289	–	0.0305	0.0321
Pr	441.53	–	116.83	80.94

Table 2 The study of grid independency for state of $Re = 50$ and $\varphi = 0.0\%$ of nanoparticles

Parameters calculated	500 × 40	45 × 700	800 × 50	900 × 55	1000 × 60
Nu_{ave}	14.034	15.082	15.98	16.321	17.101
Error/%	21.9	13.4	7	4.8	Base
$C_{f\ ave}$	0.32	0.324	0.326	0.327	0.327
Error/%	2.2	0.92	0.306	0	Base

the solid nanoparticles, base fluid and nanofluid. For calculating the effective dynamic viscosity, Brinkman equation is used [56–58]:

$$\mu_{nf} = \frac{\mu_f}{(l - \varphi)^{2.5}} \quad (17)$$

For calculating the local Nusselt number along the microchannel walls, following equation is used [59]:

$$Nu(x) = \frac{h(x) \cdot H}{k_f} \quad (18)$$

For calculating Fanning friction factor, following equation is used [60]:

$$C_f = \frac{\tau_w}{\frac{1}{2} \times \rho \times u_{in}^2} \quad (19)$$

The performance evaluation criterion [61] and the pressure drop [62, 63] between the inlet and outlet sections are calculated by following equations:

$$PEC = \frac{\left(\frac{Nu_{ave}}{Nu_{ave,\varphi=0}} \right)}{\left(\frac{f}{f_{\varphi=0}} \right)^{(1/3)}} \quad (20)$$

$$\Delta P = \bar{P}_{out} - \bar{P}_{in} \quad (21)$$

Numerical procedure and assumptions

In the present paper, the finite volume method [64–73] and the second-order discretization have been used for simulating the fluid flow and heat transfer [74, 75]. In order to couple the velocity–pressure equations in the numerical solving of this paper, SIMPLEC algorithm has been used [76, 77]. Also, for obtaining acceptable results, the maximum residual has been considered 10^{-6} [78–80]. The flow inside the microchannel is laminar, steady, Newtonian, single-phase and incompressible, and the no-slip boundary
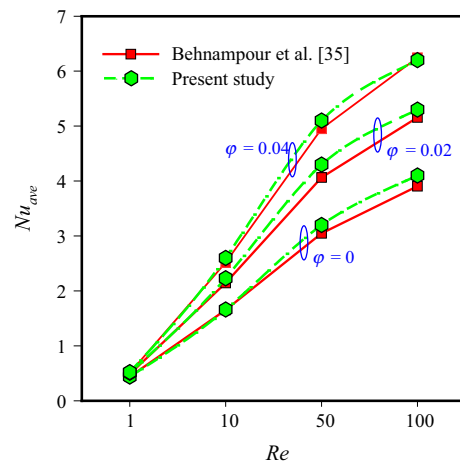

Fig. 2 The validation of present numerical investigation with the study of Behnampour et al. [35]

condition has been applied to the microchannel walls. In this simulation, the nanofluid is homogeneous and the radiation effects are negligible.

Independency from grid and validation

Table 2 indicates the demanded grid number for results independency from gridding. The selected grid number has been studied from 20,000 to 60,000 for the oil as the base fluid in Reynolds number of 50. In this investigation, the independency of flow and heat transfer parameters is intended. For the chosen grid number, the amounts of average Nusselt number and friction factor on the indented wall with rectangular ribs have been compared in different grid numbers. According to the changes of parameters in chosen grid number, it is observed that the grid number of
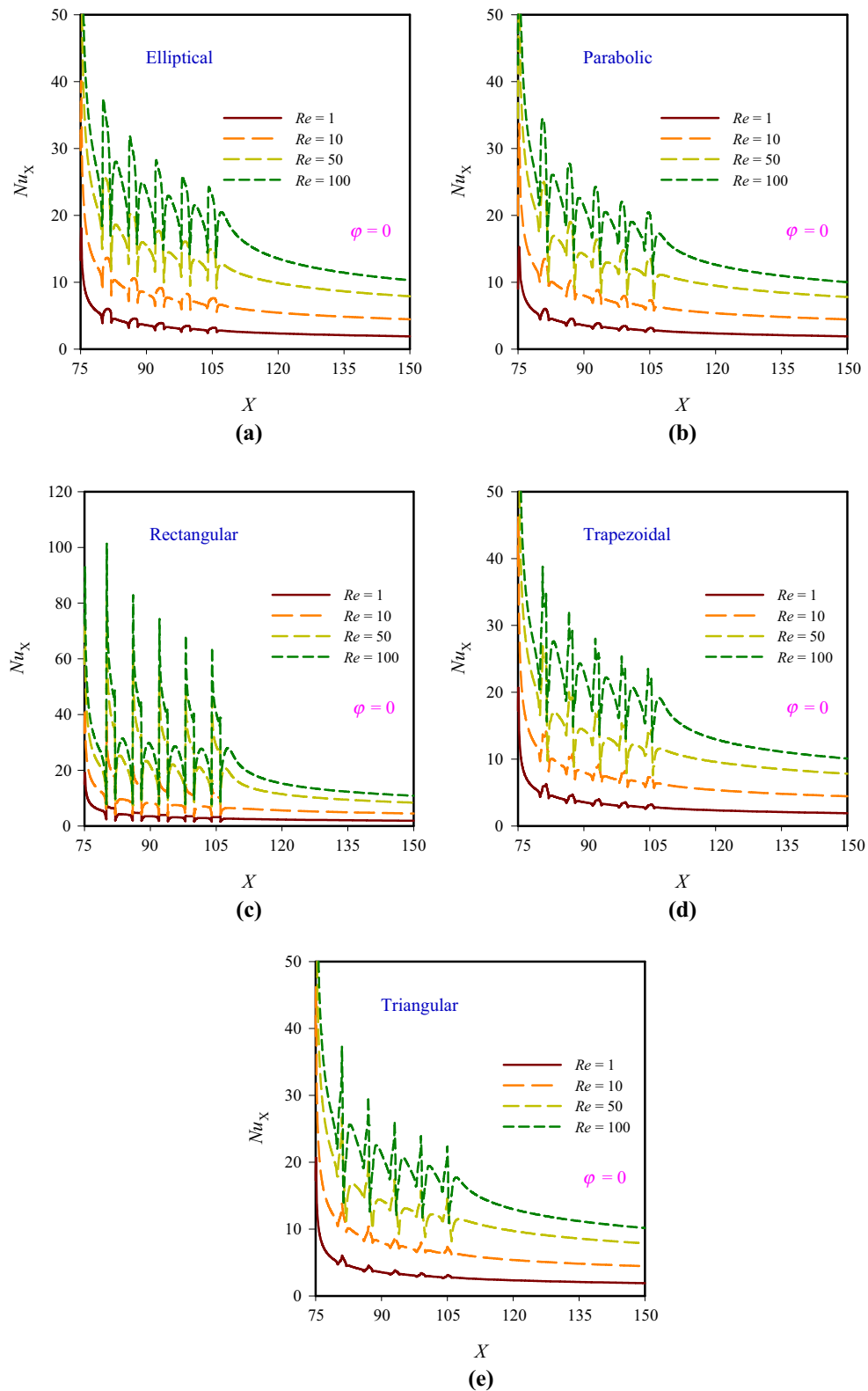
Fig. 3 The local Nusselt number figures along the indented surface for the base fluid

60,000, in comparison with less grid numbers, has more accurate results. In this research, this grid number has been used as an acceptable grid number in the simulation of numerical solving domain of heat transfer and flow.
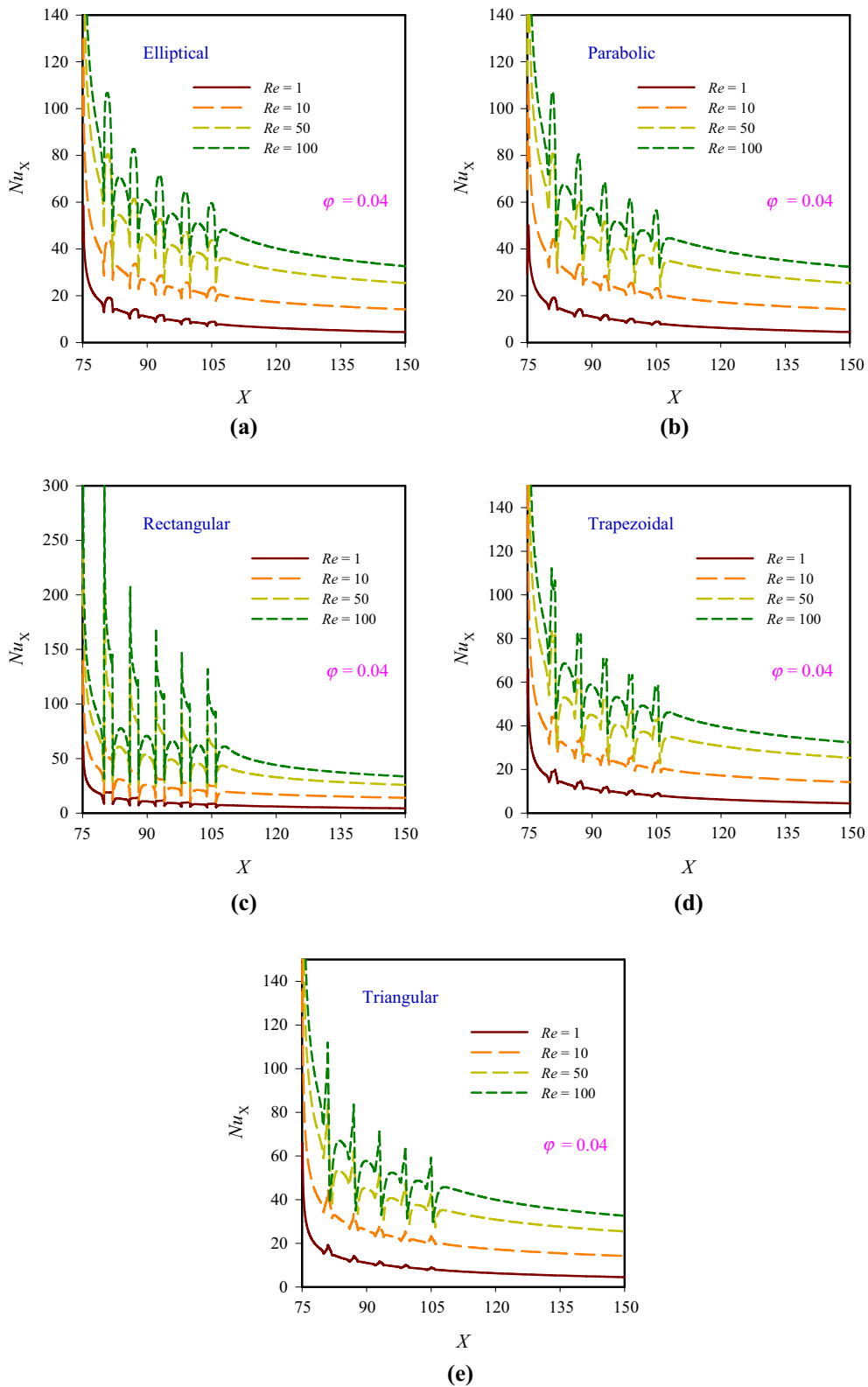
Fig. 4 The local Nusselt number figures along the indented surface for nanofluid with volume fraction of 4% of nanoparticles

Figure 2 indicates the validation of the present paper with the research of Behnampour et al. [35].

Behnampour et al. [35] numerically investigated the laminar flow of water/Ag nanofluid in a rectangular
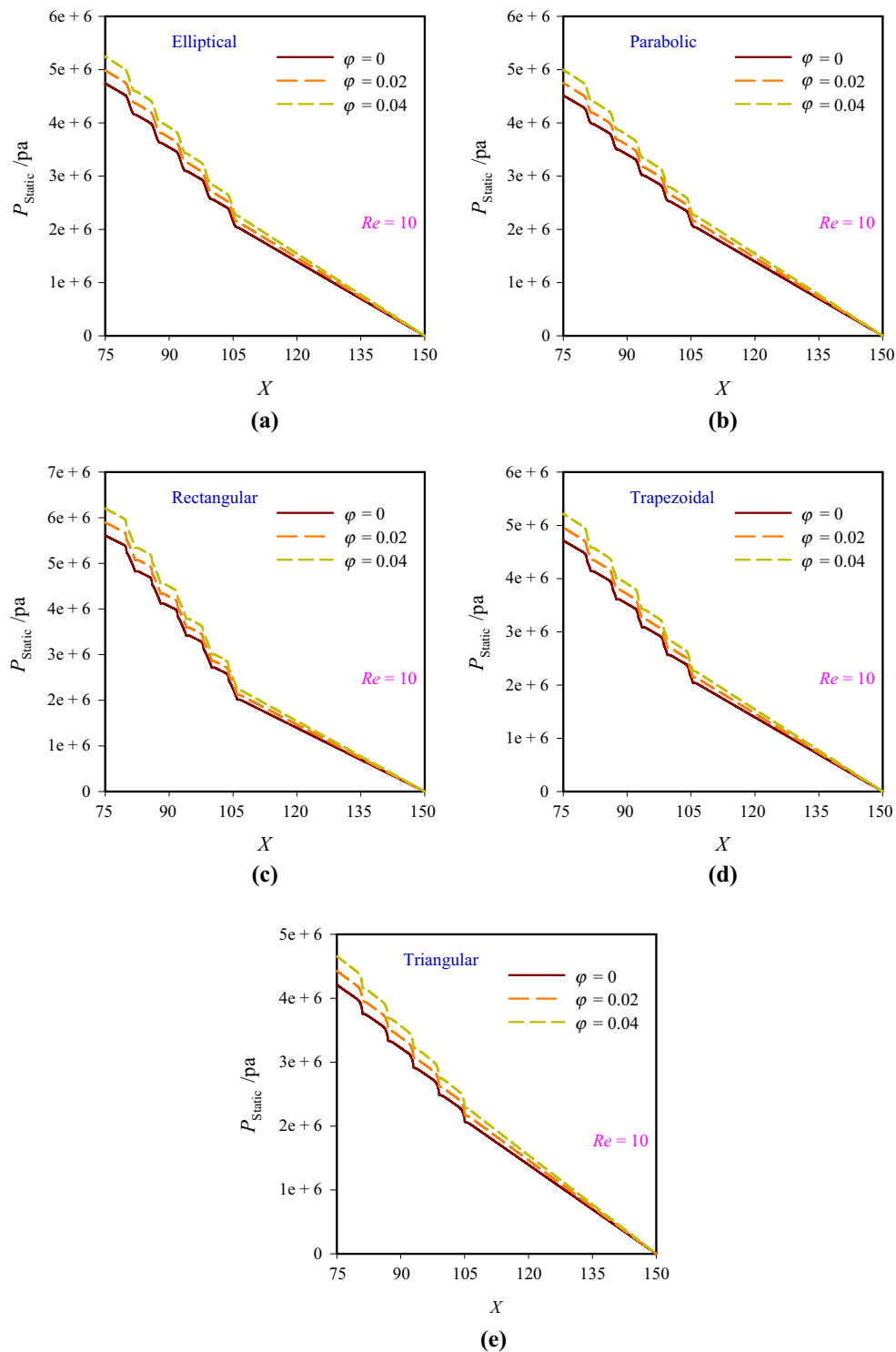
Fig. 5 The changes of pressure drop figures along the central line of flow for Reynolds number of 10

microchannel with nanoparticles volume fractions of 0–4% by using finite volume method and SIMPLEC algorithm. In Fig. 2, the numerical results of calculated average Nusselt

number on the heated wall of microchannel with rectangular ribs in Reynolds number range of 1–100 have been compared with each other. According to the coincidence of
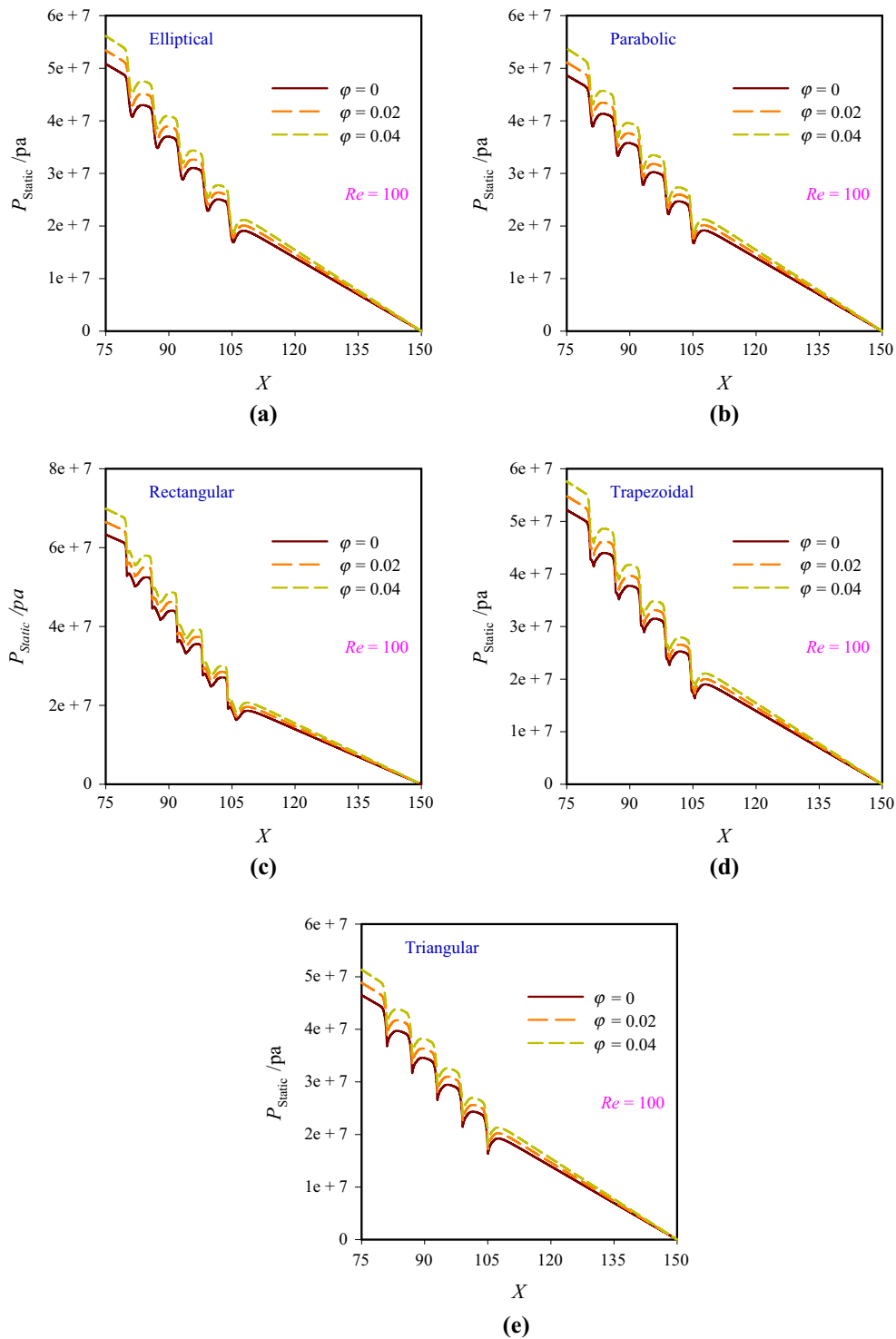
Fig. 6 The changes of pressure drop figures along the central line of flow for Reynolds number of 100

results with the numerical study of Behnampour et al. [35], the numerical solving procedure and its simulation are accurate.

Results and discussion

Figures 3 and 4 demonstrate the changes of local Nusselt number along the indented wall (hot wall) in different rib shapes and for the base fluid and nanofluid with volume
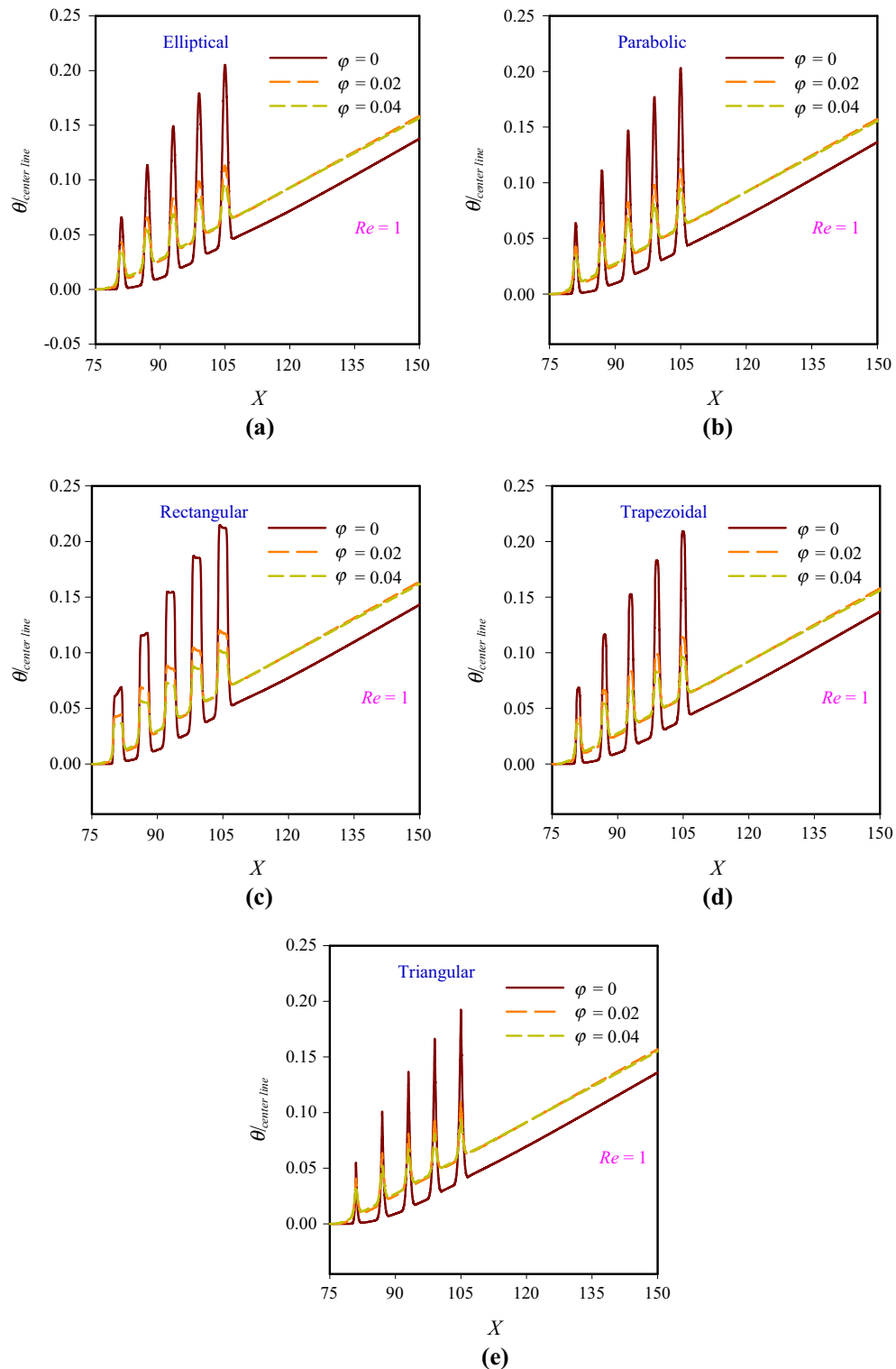
Fig. 7 The changes of dimensionless temperature figures along the central line of flow for Reynolds number of 1

fraction of 4%, respectively. Also, these figures indicate the investigation of local Nusselt number in Reynolds numbers of 1–100. Placing different rib shapes along the microchannel and on the direction of fluid motion causes

sudden changes of average Nusselt number graphs, and by increasing fluid velocity, the amount of these changes enhances. By colliding the fluid with ribs, due to the deviation of fluid direction, significant changes have been
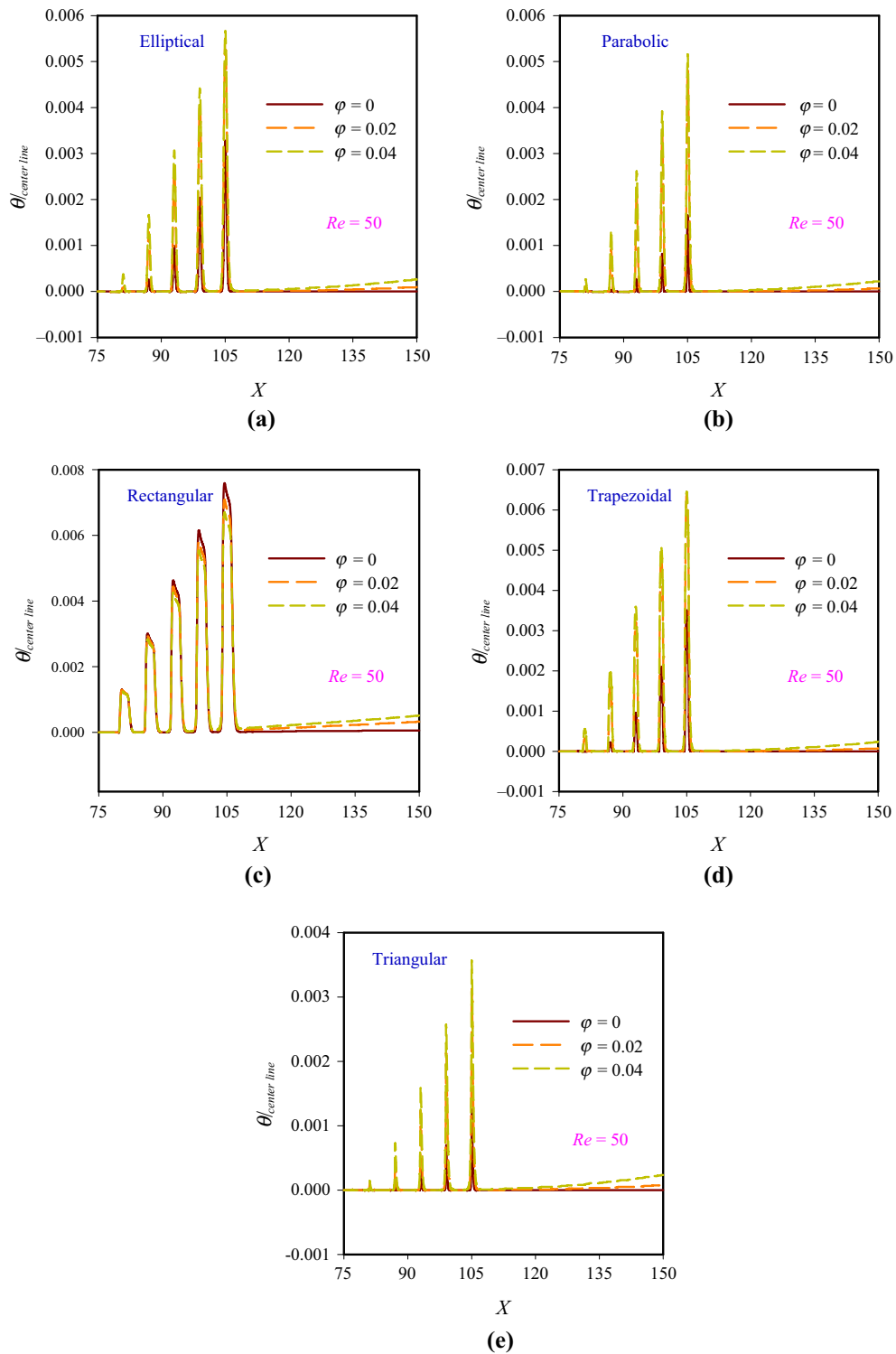
Fig. 8 The changes of dimensionless temperature figures along the central line of flow for Reynolds number of 50

created in velocity parameters, influencing the amounts of heat transfer coefficient and Nusselt number. In all of the local Nusselt number graphs, it can be observed that the maximum rate of sudden jumps in Nusselt number behavior has been seen along the primary ribs and gradually; by decreasing fluid momentum, due to the collusion of fluid with other ribs, these sudden changes are reduced. Also, the shape of ribs causes significant changes in local Nusselt number graphs; therefore, the existence of rib with sharp angles causes the most sudden changes in
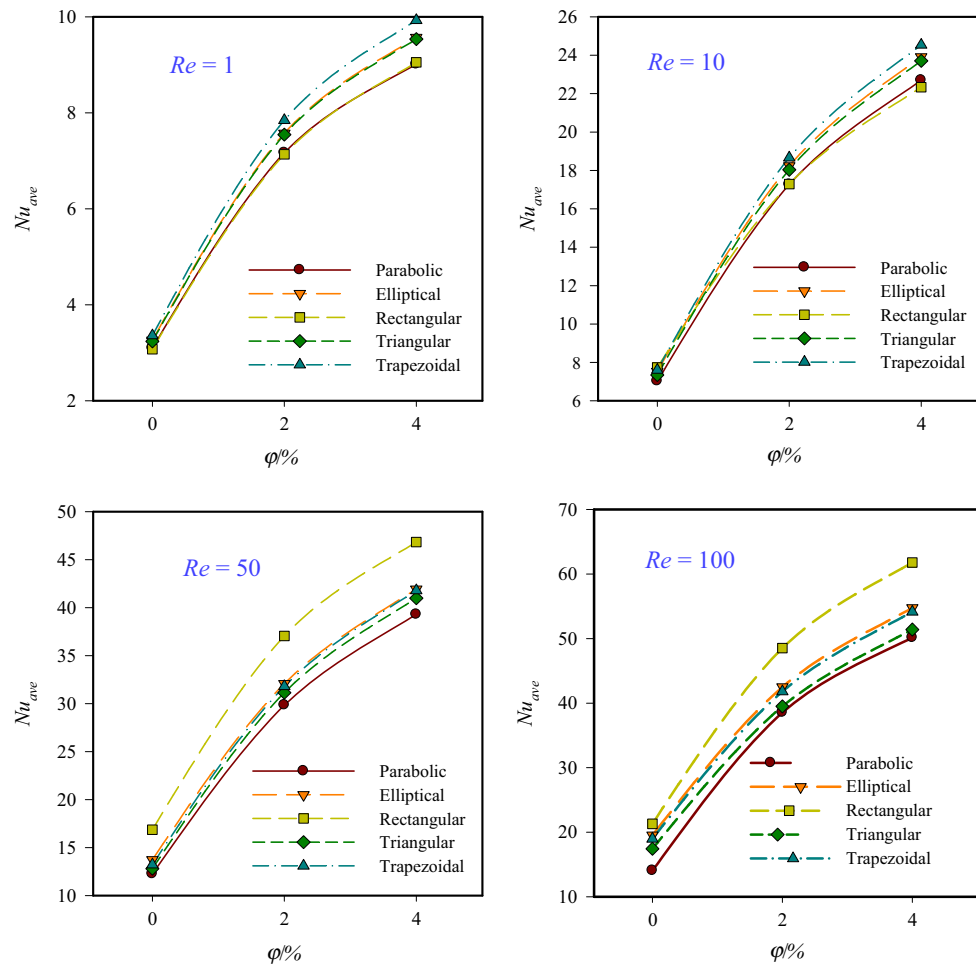
Fig. 9 The average Nusselt number figures in different rib shapes and Reynolds numbers

these figures. The existence of rib with curved surfaces causes better contact of flow with surface. According to Figs. 3 and 4, the enhancement of volume fraction and Reynolds number causes the improvement in Nusselt number. Hence, comparing to Figs. 3 and 4, it has higher level.

The changes of pressure drop along the central line of flow in Reynolds numbers of 10 and 100, and different rib shapes and volume fractions of 0, 2 and 4% of nanoparticles are demonstrated in Figs. 5 and 6, respectively. By moving the fluid among the ribs, the amount of fluid mixture improves. On the other hand, due to the encounter and contact of fluid with surface, fluid momentum decreases and this behavior causes the enhancement of pressure drop. When fluid velocity is higher, due to the augmentation of velocity changes and higher depreciation of fluid, the momentum drop increases. Also, the existence of ribs with different forms influences the hydrodynamical behavior of cooling fluid flow. The impressionability of pressure changes caused by rib shape in Reynolds number of 10, comparing to Reynolds number of 100, is less. The

main reason of this manner is because of slower motion of fluid and less changes of fluid velocity because of colliding with obstacles. Also, the enhancement of volume fraction of nanoparticle causes the augmentation of density and fluid viscosity which entails more energy drop of fluid.

Figures 7 and 8 explain the behavior of local dimensionless temperature along the central line of flow in different volume fractions of nanoparticles and rib shapes in Reynolds numbers of 1 and 50, respectively. Using ribs on hot surfaces and the collusion of fluid with ribs cause more changes in the dimensionless temperature profile at the central line of flow. In Reynolds number of 10, due to slower motion of fluid and sufficient time for heat transferring from the hot surface with the cooling fluid, the pattern of dimensionless temperature figure is somehow related to the rib shape. The increase in fluid velocity causes significant reduction in dimensionless temperature and this behavior decreases the growth of thermal boundary layer. This behavior indicates the reduction in hot surfaces impression on the central line of flow. The enhancement of volume fraction of nanoparticles and
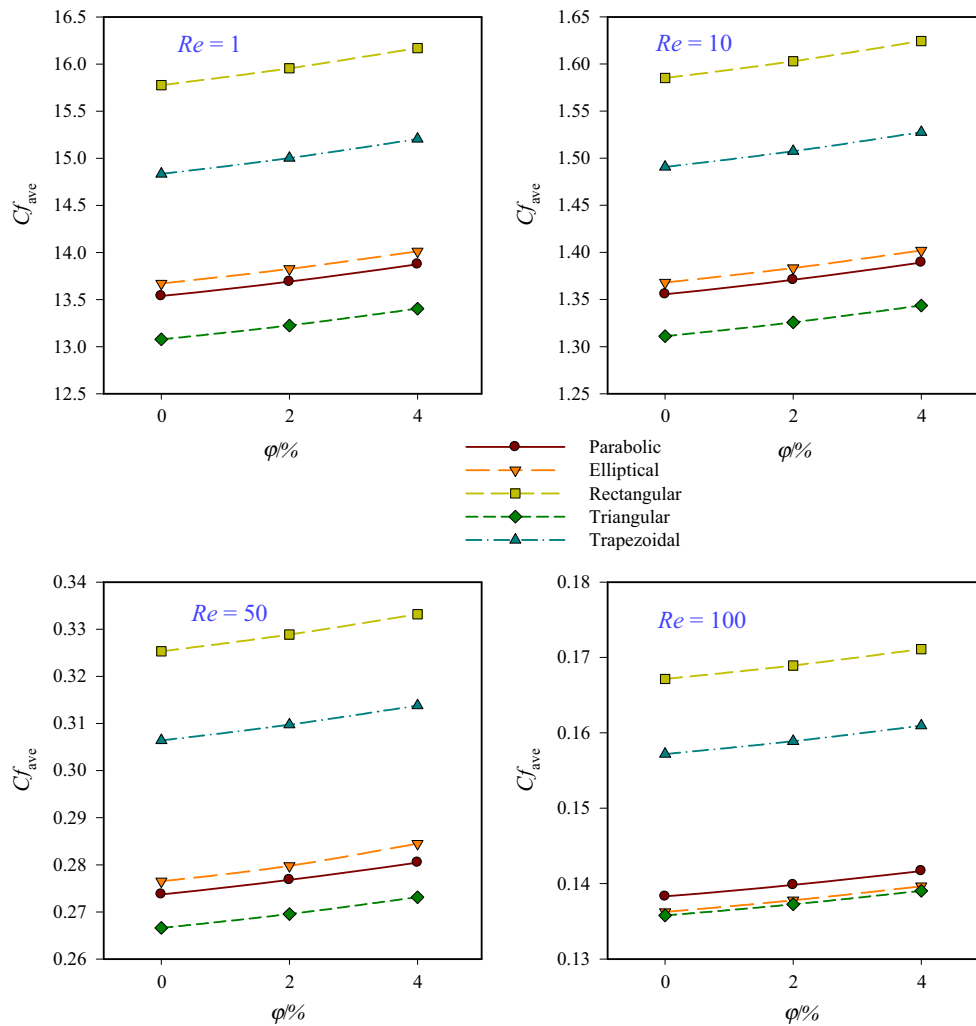
Fig. 10 The changes of average friction factor figures in different rib shapes, Reynolds numbers and volume fractions

Reynolds number entails the dominancy of inlet fluid temperature (better cooling) on the internal areas of microchannel.

Figure 9 indicates the amounts of average Nusselt number at the range of Reynolds numbers of 1–100 in volume fractions of 0, 2 and 4% of nanoparticles and different rib shapes. In the average Nusselt number figures, it can be observed that the enhancement of volume fraction of nanoparticles in the base fluid causes the improvement in conductive heat transfer coefficient and the increase in Nusselt number. This behavior is completely obvious in Reynolds numbers of 50 and 100, comparing to Reynolds numbers of 1 and 10. The increase in fluid velocity, rib shapes and geometrics causes the enhancement of convection heat transfer coefficient and Nusselt number. In Reynolds numbers of 50 and 100, the rib shape causes significant changes in heat transfer enhancement, and in Reynolds numbers of 1 and 100, there is less changes. According to the studied rib shapes, for the mathematical

numbers of 1 and 10, the maximum amount of heat transfer is related to the trapezoidal rib shape. In Reynolds numbers of 50 and 100, the sharp angles of rib cause heat transfer enhancement; therefore, in the investigated states, the rectangular rib shape has the maximum value of heat transfer. In all Reynolds numbers, the minimum amount of heat transfer is related to the parabolic rib shape. This behavior is because of the penetration of velocity gradients on the direction of fluid motion in this rib shape. Each shape of rib which can influence the disordering of thermal boundary layer has the maximum amount of Nusselt number. In Reynolds numbers of 50 and 100, after the rectangular rib, the oval, trapezoidal, triangular and parabolic rib shapes have the maximum and minimum amounts of Nusselt number, respectively.

Figure 10 demonstrates the amounts of average friction factor in different Reynolds numbers, volume fractions and rib shapes. Because of the fluid motion among the ribs, fluid momentum becomes deprecated. Also, by adding
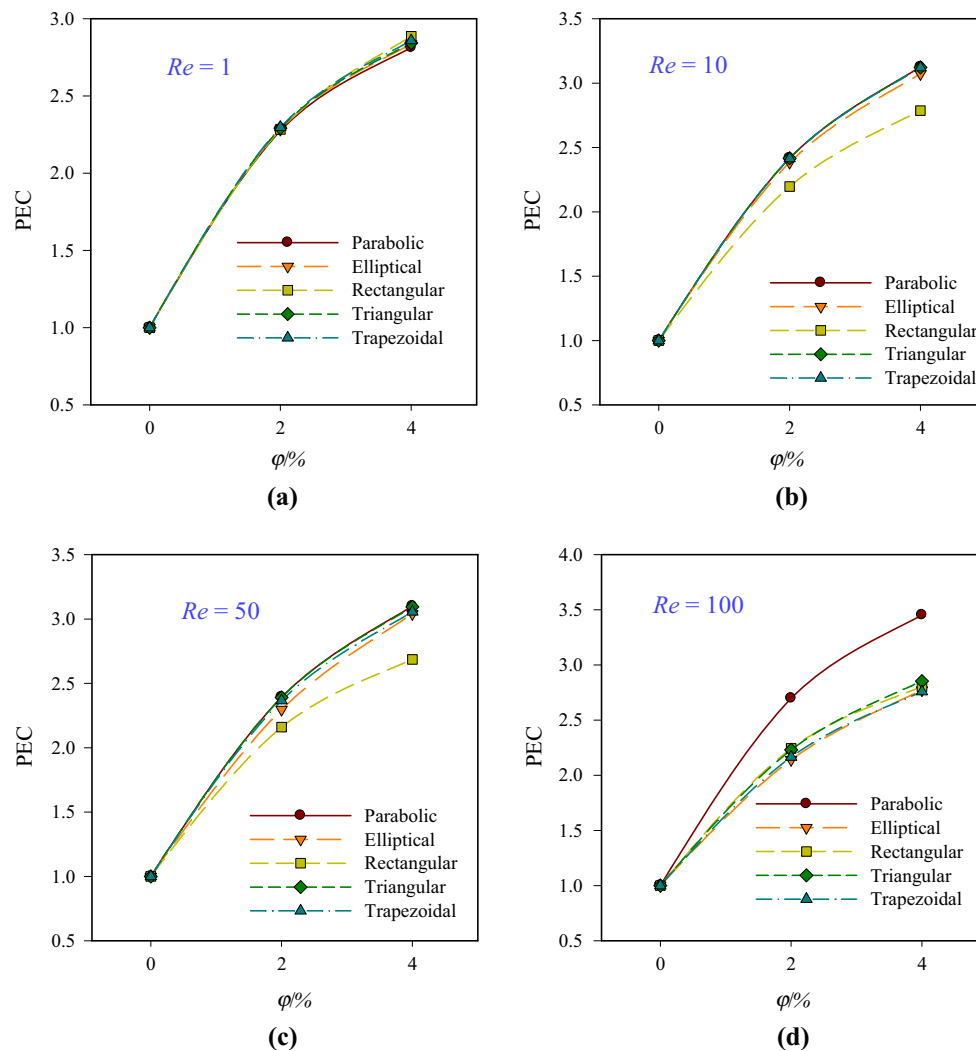
Fig. 11 The performance evaluation criterion in different rib shapes and Reynolds numbers

higher amounts of volume fractions of nanoparticles to the base fluid, due to the viscosity and higher density of cooling fluid and the contact of surface and fluid, more friction factor has been created on the internal surfaces of microchannel. On the other hand, the fluid motion on the indented surfaces causes the contact of cooling fluid with microchannel walls, and in lower Reynolds numbers, due to the slow velocity of fluid, the fluid contacts with surfaces completely. This behavior causes the fiction coefficient figures to have higher levels in Reynolds numbers of 1, comparing to other Reynolds numbers. On the other hand, by increasing Reynolds number, due to the enhancement of fluid momentum, the contact of fluid with microchannel walls does not completely happen; therefore, by increasing Reynolds number, the level of friction factor graphs reduces. Among the investigated rib shapes, the rectangular rib shape, due to the creation of the most velocity gradients on the direction of cooling fluid, has the maximum value of

friction factor. By generally observing the behavior of friction factor, it can be said that the increase in rib length and the existence of sharp angles of ribs have great influence on velocity domain; therefore, this behavior causes the increase in friction factor. In all of the studied Reynolds numbers, the rectangular, trapezoidal, oval, parabolic and triangular rib shapes have the maximum and minimum amounts of average friction factor, respectively. In the parabolic rib shape, comparing to the oval form, by increasing fluid velocity in Reynolds number of 100, the amount of average friction factor becomes more significant.

Figure 11 shows the performance evaluation criterion for different rib shapes and volume fractions of nanoparticles and Reynolds numbers of 1, 10, 50 and 100. The performance evaluation criterion is a quantitative comparison between Nusselt number and friction factor in the indented microchannel in each volume fraction, comparing
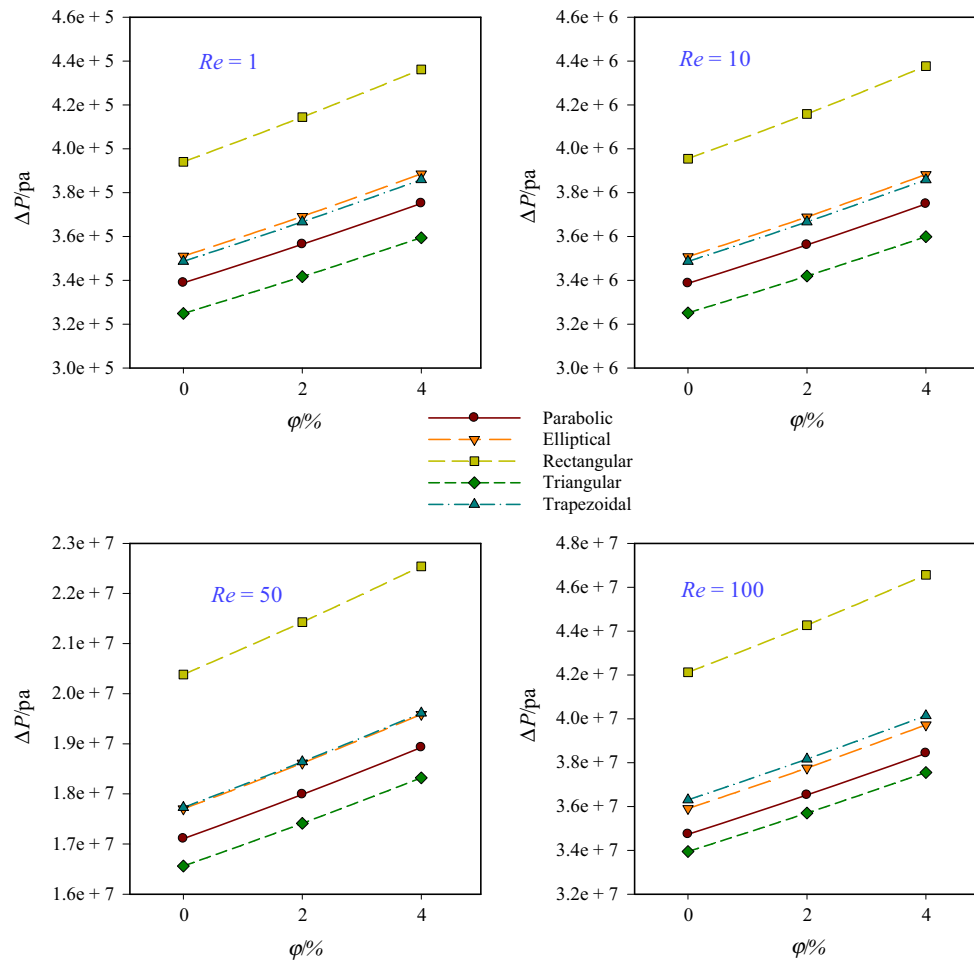
Fig. 12 The average pressure drop figures in different rib shapes and Reynolds numbers

to the pure oil as the base fluid. In all of the studied Reynolds numbers, the enhancement of fluid velocity causes significant augmentation of performance evaluation criterion. The reason of this behavior is the influence of Nusselt number and heat transfer enhancement, comparing to the friction factor enhancement, because of adding volume fraction of nanoparticles. In all of the figures, the increase in volume fraction of nanoparticles has a great effect on the enhancement of performance evaluation criterion and the figures with higher volume fractions have higher levels. Among different studied rib shapes, in Reynolds number range of 1–100, the best conformity between Nusselt number enhancements and the friction factor happens in the parabolic, triangular, trapezoidal, oval and rectangular rib shapes, respectively. Although the existence of sharp angles of the rectangular rib shape entails Nusselt number enhancement, these angles cause significant augmentation of velocity gradients in the cooling fluid and therefore cause the increase in friction factor.

Figure 12 explains the amounts of average pressure drop in the central line of flow for each different rib shape in

Reynolds number range of 1–100. These figures investigate different Reynolds numbers and volume fractions of nanoparticles, separately. The enhancement of volume fraction of nanoparticles and fluid velocity causes the increase in viscosity–density and the momentum of cooling fluid, respectively. The existence of ribs on the direction of fluid motion causes momentum damping and the reduction in kinetic energy of fluid. On the other hand, each shape of ribs which can create more velocity gradients has higher pressure drop on the direction of fluid motion and in all Reynolds numbers, and the maximum amount of pressure drop is related to the graphs with higher level of volume fraction. The behavior of pressure drop changes is similar to the behavior of average friction factor. In all of the investigated Reynolds numbers, the rectangular, trapezoidal, oval, parabolic and triangular rib shapes have the maximum and minimum amounts of average friction factor, respectively. Also, by increasing Reynolds number, the behavior of oval rib improves and its amount reduces.

Conclusions

In this research, the effect of using rectangular, oval, parabolic, triangular and trapezoidal rib shapes on the manner of laminar heat transfer of oil/MWCNT nanofluid in a two-dimensional rectangular microchannel with the length of $L = 7.5$ mm and the hydrodynamical diameter of $H = 50$ μm has been numerically investigated. The results of this research have been compared with each other in Reynolds numbers of 1, 10, 50 and 100 and different volume fractions of solid nanoparticles. The increase in volume fraction of nanoparticles and Reynolds number entails the dominancy of inlet fluid temperature (better cooling) on all of the internal areas of microchannel. The augmentation of solid nanoparticles, due to the collusion of particles with ribs, causes the enhancement of density and fluid viscosity and more energy drop of fluid. By colliding the fluid with ribs, due to the deviation of fluid direction, significant changes have been created in velocity parameters, influencing the amounts of heat transfer coefficient and Nusselt number. In the investigated states, the rectangular and parabolic ribs have the maximum and minimum amounts of average Nusselt number, respectively. Also, the rectangular, trapezoidal, oval, parabolic and triangular ribs have the maximum and minimum amounts of average friction factor, respectively. Among different studied rib shapes, in Reynolds numbers of 10, 50 and 100, the best conformity of Nusselt number enhancements and friction factor has been obtained in the parabolic, rectangular, trapezoidal, oval and rectangular rib shapes, respectively. In general, according to the importance of heat transfer enhancement methods, it is expected that the results of this research, as well as other researches in this field, be applicable and useful in today's industries such as in electronics, power stations, aerospace and automobile manufacturing.

References

1. Kasaeian A, Pourfayaz F, Bahrami L, Khodabandeh E, Yan WM. Experimental studies on the applications of PCMs and Nano-PCMs in buildings: a critical review. Energy Build. 2017;154:96–112.
2. Kavusi H, Toghraie D. A comprehensive study of the performance of a heat pipe by using of various nanofluids. Adv Powder Technol. 2017;28(11):3074–84.
3. Moraveji A, Toghraie D. Computational fluid dynamics simulation of heat transfer and fluid flow characteristics in a vortex tube by considering the various parameters. Int J Heat Mass Transf. 2017;113:432–43.
4. Rezaei M, Azimian A, Semiromi DT. The surface charge density effect on the electro-osmotic flow in a nanochannel: a molecular dynamics study. Heat Mass Transf. 2015;51:661–70.
5. Rezaei M, Azimian A, Toghraie D. Molecular dynamics study of an electro-kinetic fluid transport in a charged nanochannel based on the role of the stern layer. Phys A. 2015;426:25–34.
6. Darzi AAR, Afrouzi HH, Moshfegh A, Farhadi M. Absorption and desorption of hydrogen in long metal hydride tank equipped with phase change material jacket. Int J Hydrogen Energy. 2015;41(22):9595–610.
7. Keshavarz E, Toghraie D, Haratian M. Modeling industrial scale reaction furnace using computational fluid dynamics: a case study in Ilam gas treating plant. Appl Therm Eng. 2017;123:277–89.
8. Rabinataj AA, Afrouzi HH, Alizadeh E, Shokri V, Farhadi M. Numerical simulation of heat and mass transfer during absorption of hydrogen in metal hydride tank. Heat Transf Asian Res. 2015;46(1):75–90.
9. Noorian H, Toghraie D, Azimian A. The effects of surface roughness geometry of flow undergoing Poiseuille flow by molecular dynamics simulation. Heat Mass Transf. 2014;50:95–104.
10. Toghraie D. Numerical thermal analysis of water's boiling heat transfer based on a turbulent jet impingement on heated surface. Phys E. 2016;84:454–65.
11. Toghraie D, Mokhtari M, Afrand M. Molecular dynamic simulation of copper and platinum nanoparticles Poiseuille flow in a nanochannels. Phys E. 2016;84:152–61.
12. Farzinpour M, Rasouli S, Toghraie, DS. Experimental and numerical investigations of bubbling fluidized bed apparatus to investigate heat transfer coefficient for different fins. Comput Therm Sci Int J 2017;9(3):243–55.
13. Esfe MH, Hajmohammad H, Toghraie D, Rostamian H, Mahian O, Wongwises S. Multi-objective optimization of nanofluid flow in double tube heat exchangers for applications in energy systems. Energy. 2017;137(15):160–71.
14. Ahmadi GhR, Toghraie D. Parallel feed water heating repowering of a 200 MW steam power plant. J Power Technol. 2015;95(4):288–301.
15. Ahmadi GhR, Toghraie D, Azimian A, Akbari OA. Evaluation of synchronous execution of full repowering and solar assisting in a 200 MW steam power plant, a case study. Appl Therm Eng. 2017;112:111–23.
16. Ahmadi GHR, Akbari OA, Zarrin Ghalam M. Energy and exergy analyses of partial repowering of a natural gas-fired steam power plant. Int J Exergy. 2017;23:149.
17. Akbari OA, Marzban A, Ahmadi GhR. Evaluation of supply boiler repowering of an existing natural gas-fired steam power plant. Appl Therm Eng. 2017;124:897–910.
18. Ahmadi GhR, Toghraie D, Akbari OA. Solar parallel feed water heating repowering of a steam power plant: a case study in Iran. Renew Sustain Energy Rev. 2017;77:474–85.
19. Ahmadi GhR, Toghraie D. Energy and exergy analysis of Montazeri Steam Power Plant in Iran. Renew Sustain Energy Rev. 2016;56:454–63.
20. Ahmadi GhR, Toghraie D, Akbari OA. Efficiency improvement of a steam power plant through solar repowering. Int J Exergy. 2017;22(2):158–82.
21. Zarringhalam M, Karimipour A, Toghraie D. Experimental study of the effect of solid volume fraction and Reynolds number on heat transfer coefficient and pressure drop of CuO–water nanofluid. Exp Thermal Fluid Sci. 2016;76:342–51.
22. Choi J, Zhang Y. Numerical simulation of laminar forced convection heat transfer of Al_2O_3 water nanofluid in a pipe with return bend. Int J Therm Sci. 2012;55:90–102.
23. Afrand M, Karimipour A, Ahmadi Nadooshan A, Akbari M. The variations of heat transfer and slip velocity of FMWNT water nano-fluid along the microchannel in the lack and presence of a magnetic field. Phys E. 2016;84:474–81.

24. Manca O, Nardini S, Ricci D. A numerical study of nanofluid forced convection in ribbed channels. Appl Therm Eng. 2012;37:280–92.
25. Akbari OA, Toghraie D, Karimipour A. Numerical simulation of heat transfer and turbulent flow of water nanofluids copper oxide in rectangular microchannel with semi attached rib. Adv Mech Eng. 2016;8:1–25.
26. Safaei MR, Togun H, Vafai K, Kazi SN, Badarudin A. Investigation of heat transfer enchantment in a forward-facing contracting channel using FMWCNT nanofluids. Numer Heat Transf Part A. 2014;66:1321–40.
27. Zadeh AD, Toghraie D. Experimental investigation for developing a new model for the dynamic viscosity of Silver/Ethylene Glycol nanofluid at different temperatures and solid volume fractions. J Therm Anal Calorim. https://doi.org/10.1007/s10973-017-6696-3.
28. Esfahani NN, Toghraie D, Afrand M. A new correlation for predicting the thermal conductivity of ZnO–Ag (50–50%)/water hybrid nanofluid: an experimental study. Powder Technol. 2018. https://doi.org/10.1016/j.powtec.2017.10.025.
29. Aghanajafi A, Toghraie D, Mehmandoust B. Numerical simulation of laminar forced convection of water-CuO nanofluid inside a triangular duct. Phys E. 2017;85:103–8.
30. Sajadifar SA, Karimipour A, Toghraie D. Fluid flow and heat transfer of non-Newtonian nanofluid in a microtube considering slip velocity and temperature jump boundary conditions. Eur J Mech B Fluids. 2017;61:25–32.
31. Faridzadeh M, Semiromi DT, Niroomand A. Analysis of laminar mixed convection in an inclined square lid-driven cavity with a nanofluid by using an artificial neural network. Heat Transf Res. 2014;45:361–90.
32. Esfahani MA, Toghraie D. Experimental investigation for developing a new model for the thermal conductivity of Silica/Water–Ethylene glycol (40–60%) nanofluid at different temperatures and solid volume fractions. J Mol Liq. 2017;232:105–12.
33. Afrand M, Toghraie D, Karimipour A, Wongwises S. A numerical study of natural convection in a vertical annulus filled with gallium in the presence of magnetic field. J Magn Magn Mater. 2017;430:22–8.
34. Zadkhast M, Toghraie D, Karimipour A. Developing a new correlation to estimate the thermal conductivity of MWCNT-CuO/water hybrid nanofluid via an experimental investigation. J Therm Anal Calorim. 2017;129:859–67.
35. Behnampour A, Akbari OA, Safaei MR, Ghavami M, Marzban A, Shabani GAS, Zarringhalam M, Mashayekhi R. Analysis of heat transfer and nanofluid fluid flow in microchannels with trapezoidal, rectangular and triangular shaped ribs. Phys E. 2017;91:15–31.
36. Akbari OA, Karimipour A, Toghraie D, Safaei MR, Alipour Goodarzi MH, Dahari M. Investigation of Rib's height effect on heat transfer and flow parameters of laminar water–Al2O3 nanofluid in a two dimensional rib-microchannel. Appl Math Comp. 2016;290:135–53.
37. Akbari OA, Karimipour A, Toghraie D, Karimipour A. Impact of ribs on flow parameters and laminar heat transfer of Water–Aluminum oxide nanofluid with different nanoparticle volume fractions in a three-dimensional rectangular microchannel. Adv Mech Eng. 2016;7:1–11.
38. Karimipour A, Alipour H, Akbari OA, Semiromi DT, Esfe MH. Studying the effect of indentation on flow parameters and slow heat transfer of water–silver nano-fluid with varying volume fraction in a rectangular two-dimensional micro channel. Indian J Sci Technol. 2016;8:2015.
39. Gravndyan Q, Akbari OA, Toghraie D, Marzban A, Mashayekhi R, Karimi R, Pourfattah F. The effect of aspect ratios of rib on the heat transfer and laminar water/TiO2 nanofluid flow in a two-dimensional rectangular microchannel. J Mol Liq. 2017;236:254–65.
40. Akbari OA, Toghraie D, Karimipour A, Marzban A, Ahmadi GR. The effect of velocity and dimension of solid nanoparticles on heat transfer in non-Newtonian nanofluid. Phys E. 2017;86:68–75.
41. Yari Ghale Z, Haghshenasfard M, Nasr Esfahany M. Investigation of nanofluids heat transfer in a ribbed microchannel heat sink using single-phase and multiphase CFD models. Int Commun Heat Mass Transf. 2015;68:122–9.
42. Sarlak R, Yousefzadeh Sh, Akbari OA, Toghraie D, Sarlak S, Assadi F. The investigation of simultaneous heat transfer of water/Al2O3 nanofluid in a close enclosure by applying homogeneous magnetic field. Int J Mech Sci. 2017;133:674–88.
43. Parsaiemehr M, Pourfattah F, Akbari OA, Toghraie D, Sheikhzadeh Gh. Turbulent flow and heat transfer of water/Al2O3 nanofluid inside a rectangular ribbed channel. Phys E. 2018;96:73–84.
44. Li YF, Xia GD, Ma DD, Jia YT, Wang J. Characteristics of laminar flow and heat transfer in microchannel heat sink with triangular cavities and rectangular ribs. Int J Heat Mass Transf. 2016;98:17–28.
45. Andreozzi A, Manca O, Nardini S, Ricci D. Forced convection enhancement in channels with transversal ribs and nanofluids. Appl Therm Eng. 2016;98:1044–53.
46. Mashayekhi R, Khodabandeh E, Bahraei M, Bahrami L, Toghraie D, Akbari OA. Application of a novel conical strip insert to improve the efficacy of water–Ag nano-fluid for utilization in thermal systems: a two-phase simulation. Energ Conv Manag. 2017;151:573–86.
47. Toghraie D, Davood Abdollah MM, Pourfattah F, Akbari OA, Ruhani B. Numerical investigation of flow and heat transfer characteristics in smooth, sinusoidal and zigzag-shaped microchannel with and without nano-fluid. J Therm Anal Calorim. 2017. https://doi.org/10.1007/s10973-017-6624-6.
48. Pourfattah F, Motamedian M, Sheikhzadeh Gh, Toghraie D, Akbari OA. The numerical investigation of angle of attack of inclined rectangular rib on the turbulent heat transfer of water–Al2O3 nanofluid in a tube. Int J Mech Sci. 2017;131–132:1106–16.
49. Mehdi Derakhshan M, Akhavan-Behabadi MA. Mixed convection of MWCNTeheat transfer Oil nanofluid inside inclined plain and microfin tubes under laminar assisted flow. Int J Therm Sci. 2016;99:1–8.
50. Raisia A, Aminossadati SM, Ghasemi B. An innovative nanofluid-based cooling using separated natural and forced convection in low Reynolds flows. J Taiwan Ins Chem Eng. 2016;62:259–66.
51. Aminossadati SM, Raisi A, Ghasemi B. Effects of magnetic field on nanofluid forced convection in a partially heated microchannel. Int J Non-Lin Mech. 2011;46:1373–82.
52. Raisi A, Ghasemi B, Aminossadati SM. A numerical study on the forced convection of laminar nanofluid in a microchannel with both slip and No slip condition. Numer Heat Transf A Appl. 2011;59:114–29.
53. Alipour H, Karimipour A, Safaei MR, Semiromi DT, Akbari OA. Influence of T-semi attached rib on turbulent flow and heat transfer parameters of a silver–water nanofluid with different volume fractions in a three-dimensional trapezoidal microchannel. Phys E. 2016;88:60–76.
54. Akbari OA, Goodarzi M, Safaei MR, Zarringhalam M, Shabani GAS, Dahari M. A modified two-phase mixture model of nanofluid flow and heat transfer in 3-d curved microtube. Adv Powder Tech. 2016;27:2175–85.
55. Chon CH, Kihm KD, Lee SP, Choi SUS. Empirical correlation finding the role of temperature and particle size for nanofluid (Al2O3) thermal conductivity enhancement. Appl Phys Lett. 2005;87:153107–153107-3.
56. Brinkman H. The viscosity of concentrated suspensions and solutions. J Chem Phys. 1952;20:571. https://doi.org/10.1063/1.1700493.

57. Akbari OA, Afrouzi HH, Marzban A, Toghraie D, Malekzade H, Arabpour A. Investigation of volume fraction of nanoparticles effect and aspect ratio of the twisted tape in the tube. J Therm Anal Calorim. 2017. https://doi.org/10.1007/s10973-017-6372-7.

58. Heydari M, Toghraie M, Akbari OA. The effect of semi-attached and offset mid-truncated ribs and water/TiO$_2$ nanofluid on flow and heat transfer properties in a triangular microchannel. Therm Sci Eng Prog. 2017;2:140–50.

59. Sheikholeslami M, Gorji-Bandpy M, Ganji DD. Effect of discontinuous helical turbulators on heat transfer characteristics of double pipe water to air heat exchanger. Energy Convers Manag. 2016;118:75–87.

60. M Safaei MR. Gooarzi M. Akbari OA. Safdari Shadloo M. Dahari M. Performance evaluation of nanofluids in an inclined ribbed microchannel for electronic cooling applications, "electronics cooling" In: Sohel Murshed SM editor. InTech, 2016. https://doi.org/10.5772/62898. Available from: http://www.intechopen.com/books/electronics-cooling/performance-evaluation-of-nanofluids-in-an-inclined-ribbed-microchannel-for-electronic-cooling-appli.

61. Chai L, Xia G, Zhou M, Li J, Qi J. Optimum thermal design of interrupted microchannel heat sink with rectangular ribs in the transverse microchambers. Appl Therm Eng. 2013;51:880–9.

62. Shamsi MR, Akbari OA, Marzban A, Toghraie D, Mashayekhi R. Increasing heat transfer of non-Newtonian nanofluid in rectangular microchannel with triangular ribs. Phys E. 2017;93:167–78.

63. Vanaki SM, Mohammed HA. Numerical study of nanofluid forced convection flow in channels using different shaped transverse ribs. Int Commun Heat Mass Transf. 2015. https://doi.org/10.1016/j.icheatmasstransfer.2015.07.004.

64. Safaei MR, Saleh SR, Goodarzi M. Numerical studies of laminar natural convection in a square cavity with orthogonal grid mesh by finite volume. Int J Adv Des Manuf Technol (Majl J Mech Eng). 2008;1(2):13.

65. Moghiman M, Rahmanian B, Safaei MR, Goodarzi M. Numerical investigation of heat transfer in circular perforated plates exposed to parallel flow and suction. Int J Adv Des Manuf Technol (Majl J Mech Eng). 2008;1(3):43.

66. Seifia AR, Akbari OA, Alrashed AAAA, Afshary F, Ahmadi Sheikh Shabani Gh, Seifi R, Goodarzi M, Pourfattah F. Effects of external wind breakers of Heller dry cooling system in power plants. Appl Therm Eng. 2018. https://doi.org/10.1016/j.applthermaleng.2017.10.118.

67. Maghmoumi Y, Alavi MA, Safaei MR, Nourollahi I. Numerical analyses of steady non-Newtonian flow over flat plate on intermediate reynolds numbers by finite volume method. Int J Adv Des Manuf Technol (Majl J Mech Eng). 2008;1(4):21.

68. Nourollahi I, Zafarmand B, Safaei MR, Maghmoumi Y. An investigation of lid driven cavity flow by using large eddy simulation. Int J Adv Des Manuf Technol (Majl J Mech Eng). 2008;2(1):25.

69. Safaei MR, Goshayshi HR. Numerical Simulation of Laminar and Turbulent Mixed Convection in Rectangular Enclosure with Hot upper Moving Wall. Int J Adv Des Manuf Technol (Majl J Mech Eng). 2010;3(2):49.

70. Safaei MR, Goodarzi M, Mohammadi M. Numerical modeling of turbulence mixed convection heat transfer in air filled enclosures by finite volume method. Int J Multiphys. 2011;5(4):307–24.

71. Karimipour A, Afrand M, Akbari M, Safaei MR. Simulation of fluid flow and heat transfer in the inclined enclosure. Int J Mech Aerosp Eng. 2012;2012(6):86–91.

72. Safaei MR, Goshayshi HR, Saeedi Razavi B, Goodarzi M. Numerical investigation of laminar and turbulent mixed convection in a shallow water-filled enclosure by various turbulence methods. Sci Res Essay. 2011;6(22):4826–38.

73. Safaei MR, Rahmanian B, Goodarzi M. Numerical study of laminar mixed convection heat transfer of power-law non-Newtonian fluids in square enclosures by finite volume method. Int J Phys Sci. 2011;6(33):7456–70.

74. Khodabandeh E, Rahbari A, Rosen MA, Ashrafi ZN, Akbari OA, Anvari AM. Experimental and numerical investigations on heat transfer of water-cooled lance for blowing oxidizing gas in electrical arc furnace. Energ Conv Manag. 2017;148:43–56.

75. Khodabandeh E, Abbasi A. Performance optimization of water–Al$_2$O$_3$ nanofluid flow and heat transfer in trapezoidal cooling microchannel using constructal theory and two phase Eulerian–Lagrangian approach. Powder Technol. 2018;323:103–14.

76. Arani AAA, Akbari OA, Safaei MR, Marzban A, Alrashed AAAA, Ahmadi GR, Nguyen TK. Heat transfer improvement of water/single-wall carbon nanotubes (SWCNT) nanofluid in a novel design of a truncated double layered microchannel heat sink. Int J Heat Mass Transf. 2017;113:780–95.

77. Khodabandeh E, Pourramezan M, Pakravan MH. Effects of excess air and preheating on the flow pattern and efficiency of the radiative section of a fired heater. Appl Therm Eng. 2016;105:537–48.

78. Rezaei O, Akbari OA, Marzban A, Toghraie D, Pourfattah F, Mashayekhi R. The numerical investigation of heat transfer and pressure drop of turbulent flow in a triangular microchannel. Phys E. 2017;93:179–89.

79. Rezaei M, Azimian AR, Toghraie D. Molecular dynamics study of an electro-kinetic fluid transport in a charged nanochannel based on the role of the stern layer. Phys A Stat Mech Appl. 2015;426:25–34.

80. Rezaei M, Azimian AR, Toghraie D. The surface charge density effect on the electro-osmotic flow in a nanochannel: a molecular dynamics study. Heat Mass Transf. 2015;51(5):661–70.